

See discussions, stats, and author profiles for this publication at: <https://www.researchgate.net/publication/233553105>

Estimating Waveguide Model Elements from Acoustic Tube Measurements

Article in *Acta Acustica united with Acustica* · November 2009
DOI: 10.3813/AAA.918241

CITATIONS
15

READS
228

2 authors:



Tamara Smyth
University of California, San Diego
52 PUBLICATIONS 201 CITATIONS



SEE PROFILE



Jonathan Abel
Stanford University
150 PUBLICATIONS 3,989 CITATIONS

SEE PROFILE

Some of the authors of this publication are also working on these related projects:

-  **Saxophone fingerings Identification and modeling** [View project](#)
-  **Artificial Reverberation** [View project](#)

Estimating Waveguide Model Elements from Acoustic Tube Measurements

Tamara Smyth

School of Computing Science, Simon Fraser University, 250-13450 102nd Ave., Surrey BC V3T 0A3, Canada.
tamaras@cs.sfu.ca

Jonathan S. Abel

Center for Computer Research in Music and Acoustics (CCRMA), Dept. of Music, Stanford University, Stanford, California 94305-8180. abel@ccrma.stanford.edu

Summary

One-dimensional digital waveguides are widely used to model traveling pressure waves along wind instrument bores comprised of concatenated cylindrical or conical sections. Waveguide filter elements model frequency-dependent losses and delay (dispersion) occurring during propagation and at any boundary or discontinuity producing reflected and transmitted waves. In this work, a technique is described for estimating wind instrument waveguide elements from several measurements of the system's impulse response, each measurement taken with the system having incrementally varying termination/boundary conditions. The measured impulse responses yield sequences of multiple arrivals from which estimates of waveguide element transfer functions may be formed. The measurement and post signal processing technique is explored using simple structures consisting of cylindrical and conical tubes, as these are well described theoretically and provide a basis for validating measured data. All waveguide elements necessary for modeling typical wind instrument bores are collected here, each presented with a theoretical description and accompanying measurement. The measurement and processing system is then shown to yield data closely matching the theory, thus providing confidence that the technique may be extended to accurately measure structures which are more difficult to describe theoretically, such as an instrument's flaring bell.

PACS no. 43.75.Wx, 43.75.Yy, 43.75.Zz

1. Introduction

Computer simulations involving wave propagation in one dimension often make use of the digital waveguide, or bi-directional delay line [1]. The theory of digital waveguide synthesis and its use in modeling musical instruments is well documented [1, 2, 3]. It is a particularly practical synthesis technique for real-time interactive computer music instruments as it is computationally efficient, with musically relevant control parameters easily changed in real time.

When modeling wind instrument bores that are cylindrical and/or conical, a waveguide section is used, incorporating a pure delay corresponding to the length (or desired fundamental frequency) of the bore and digital filters to account for losses and dispersion of the propagating wave, such as due to viscous drag and thermal conduction occurring along the bore walls [4, 5, 6]. Additional filtering is required at waveguide section boundaries, such as an open or closed termination, or a junction with one or

more waveguide sections, as these change the characteristic wave impedance and result in a reflection and a complementary transmission of the wave. Waveguide models of acoustic tubes and musical instrument bores therefore comprise three types of waveguide elements: 1) a waveguide section, modeling bore wave propagation and loss, 2) a termination, modeling bore end conditions, and 3) a scattering junction, modeling the bore scattering, as in the connection of waveguide sections.

Depending on the shape of the bore being modeled, a one-dimensional digital waveguide model may not be sufficiently accurate since the waveguide section models only planar or spherical wave propagation in cylindrical or conical tubes, respectively. That is, instruments departing from these simple shapes, such as the flared opening of many brass instruments, generate continuous reflection and transmission of the propagating wave that must either be modeled using a piecewise connection of several waveguide sections corresponding to the instrument's contour, or by obtaining the bore's (or bore section's) measured or theoretical reflection function.

If a measured reflection function of an entire instrument body is used in the context of a real-time parametric model, further processing will be necessary to separate

Received 16 February 2009,
accepted 13 July 2009.

components of the response that can be made parametric. For example, in work by Rodet and Vergez [7], the downstream pressure of a lip-reed model is obtained by convolving the input bore pressure with the measured reflection function of a trumpet bore and bell, with the delay corresponding to the length of the trumpet's cylindrical section made variable according to the user's desired sounding frequency. This would be equivalent to a waveguide model having a single cylindrical waveguide section with a reflection function corresponding to the non-cylindrical segment of the measurement.

Several techniques exist for measuring acoustic properties of tubes and wind instrument bores, each one developed for obtaining the acoustic information required for a particular application. Probably most notable and common among the acoustics community are techniques for obtaining the bore's input impedance as a function of frequency [8, 9, 10, 11], as this measurement fully characterizes the instrument and may be used to obtain its resonances as well as to estimate its area function, as was done for the vocal tract [12]. Though the input impedance of a tube is closely related to its impulse response, since a change of impedance results in reflection and transmission of the propagating wave, it is not as easily incorporated into a waveguide model because it describes the acoustics of the whole instrument, not the behavior of individual sections and elements comprising the model. This may be problematic (though not necessarily insurmountable) from an instrument design point of view, when it is desirable to leave the model's control parameters intact.

Perhaps more relevant to the work presented here are the time-domain techniques for obtaining reflection transfer functions of instrument bores or bore sections. Agulló *et al.* [13] present a system for measuring the reflection function of a discontinuity in a divergent "cylindroconical" acoustic tube. Here, two diametrically opposed microphones—the sum of their signals eliminating undesired higher-order modes with an odd number of diametral nodal lines—are placed at sufficient distance from the discontinuity and the driver that a measurement of a short pulse-like excitation, followed by its reflection off the discontinuity, can be made before overlapping with any other reflections in the system setup.

In work by Välimäki *et al.* [14] a measurement technique is presented in which two microphones are placed at a distance from one another along the length of the bore such that right and left (incident and reflected) travelling waves may be separated to estimate propagation loss and reflection at a tube's open end. The work mentions the difficulties involved in driving the system with a pulse and the necessity for considering the transfer function of the speaker when producing a driving signal that is a "perfect" impulse. In their method, an impulse is sent to the driver, the response is recorded, and the driving impulse is then computed using inverse filtering.

In another common measurement technique referred to as acoustic pulse reflectometry [15], a pulse drives a sufficiently long source tube to which an instrument is affixed,

with reflections from the instrument being recorded without interference from any reflections in the source tube. As with the input impedance curves discussed above—in fact this technique is often used to obtain input impedance curves—this measurement is used to describe the properties of the complete tube using a single round-trip propagation of the excitation signal along its length—not of single waveguide elements.

In methods using a pulse as the excitation signal, there are trade offs between the width of the pulse being sent down the tube, the length of the reflected signal, the SNR and the covered bandwidth. Though a loud narrow pulse is desirable, both for having sufficient energy to excite the system above the noise floor and to cover a broader frequency bandwidth, such a pulse can cause the speaker to distort. Sufficient energy may be applied to the system by making the pulse longer. A wider pulse has a reduced bandwidth and restricts placement of the microphones, which need to be sufficiently spaced to avoid interference between incident and reflected pulses.

It should be noted that it has become increasingly common practice to use excitation signals such as a swept sinusoid, essentially an impulse smeared in time, as this has sufficient energy to excite the system above the noise floor without causing the distortion that would inevitably result from using an impulse with similar energy [16]. All the techniques above could likely be improved using the swept-sine technique, with mathematical post-processing leading to an excitation signal that is essentially a pulse. In so doing, the duration of the input signal is completely divorced from the effective pulse sent out the drive. That is, regardless of the choice of swept-sine length, the input driving signal will always be post-processed so its effective length is that of an impulse filtered by the speaker transfer function.

In an additional multiple microphone technique to the one cited above, Antoine Lefebvre *et al.* [17, 18] position multiple microphones along the length of the bore and excite the system with white noise, providing sufficient energy to obtain as good a SNR as if using a swept sinusoid. By analyzing the signals simultaneously received at each of the microphones, the left and right going wave may be separated and the reflection function inferred. The disadvantage of this system as compared to the work presented here is that it uses multiple microphones, requiring separate processing for different frequency bands: the further spaced microphones give information on low frequencies while the closer microphones give information on high frequencies. Though certainly a reasonable technique, there is the added task of calibrating the microphones and piecing together the processing results from different frequency bands, requiring less straight forward signal processing.

In this work, an acoustic measurement and signal processing technique is presented which allows the complete system impulse response—the sequence of multiple arrivals from the tube and not just its single round-trip reflection function—to be interpreted in the time domain

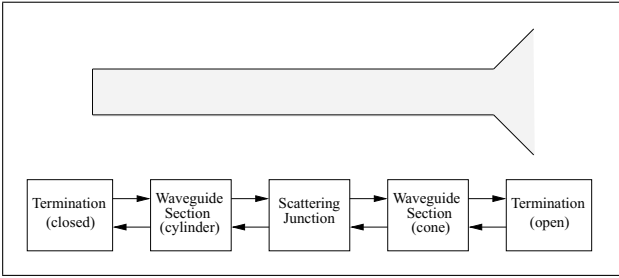


Figure 1. Example waveguide model of the open cylicone showing an example application of three waveguide elements.

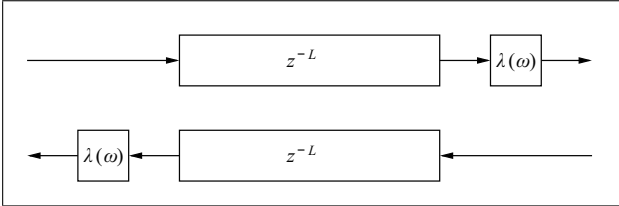


Figure 2. A waveguide section showing a pure delay of M samples corresponding to a physical length L , and frequency-dependent propagation losses $\lambda(\omega)$, which account for magnitude attenuation and phase velocity (dispersion).

and used for estimating waveguide model element transfer functions. Here, measurements are made incrementally on four tube structures, each one specially designed and built to yield a measurement corresponding to an additional waveguide element leading to the final structure, a cylinder with an attached cone, henceforth referred to as a *cylicone* (Figure 1). Though it would certainly be possible to estimate the input impedance from the measurements presented here, it is not the aim of this work. Rather, the focus is on analyzing and interpreting the information contained within a sequence of impulse arrivals—an in-depth discussion of the time-domain impulse response waveform typically omitted from the literature—and using the results to estimate filter components of a waveguide model.

The measurement setup has the benefit of being extremely simple, requiring only a single microphone and a co-located speaker at one end of the tube (the placement remains the same for each tube structure and for each waveguide element being estimated) as well as a full duplex audio device capable of simultaneously sending and receiving a signal. This eliminates the need to calibrate multiple microphones and, since the swept-sine excitation technique is used, provides more accurate and distortion-free measurements. In addition, because the placement of the speaker and microphone is at one end of the tube, the location of the mouthpiece in most western wind instruments, the measured impulse responses can be directly incorporated into a reed model requiring a value for the downstream (bore) pressure to determine the reed’s overall driving force [19].

The measurements are validated (as one must be certain a measurement technique is yielding expected data free of unexplained artifacts) using four tube structures comprising cylinders and cones, as the theory for these shapes

is well known and provides a good basis for comparison with the estimated element transfer functions. If measurements yield data showing good agreement with theory for these shapes, it suggests that the technique can be easily extended to include shapes that are much more difficult to account for theoretically.

Section 2 serves to collect the theory describing waveguide elements. In addition to forming the theoretical basis for assessing the quality of the proposed measurement technique, this also provides a single source for wind instrument waveguide element design. Section 3 presents the measurement technique and setup used to obtain the impulse responses from which waveguide element transfer functions may be estimated. Section 4 presents the measured data corresponding to the four tube structures, describes the estimation of each waveguide element, and compares the measured and theoretically predicted waveguide element transfer functions, shown to have very good agreement. The detailed illustration and discussion of the waveguide elements observed within the echo responses of the four impulse responses facilitates the discussion of the signal processing required to isolate and estimate each waveguide element transfer function.

2. Waveguide theory

2.1. The waveguide section: wave propagation

The digital waveguide, or bidirectional delay line, implements d’Alembert’s solution for plane waves propagating along a lossless cylindrical tube,

$$y(t, x) = y^+(t - x/c) + y^-(t + x/c), \tag{1}$$

where the positive and negative superscripts indicate travelling pressure waves y moving in opposite directions, t and x are the time and spatial variables, respectively, and c is the propagation speed. Spherical waves in conical tubes may be similarly modeled as they are the sum of traveling waves moving toward and away from the cone apex. Due to spherical spreading, waves propagating from a distance r_0 from the cone apex, to a distance r_1 from the cone apex, will experience a pressure scaling of r_0/r_1 .

The digital waveguide, Figure 2, is equivalent to sampling (1), where the delay in samples M is proportional to the tube section length L . In practice, it is also useful to account for frequency-dependent propagation losses, with transfer function having both a magnitude and phase response, arriving from viscous drag and thermal conduction along the tube walls. The propagation constant per unit length is given by

$$\Gamma(\omega) = \alpha(\omega) + j \frac{\omega}{v(\omega)}, \tag{2}$$

where $\alpha(\omega)$ is the attenuation coefficient, $v(\omega)$ is the phase velocity, and ω is the angular frequency [4]. The attenuation and phase delay over a tube of length L is then given by

$$\exp \left[-\Gamma(\omega)L \right].$$

Table I. Molecular constants evaluated at 26.85°C, as provided by [4].

	Symbol	Values	Units
Air density	ρ	1.18×10^{-3}	g/cm^2
Viscosity	η	1.85×10^{-4}	g/(s cm)
(Prandtl) $^{\frac{1}{2}}$	ν	0.841	
Ratio of specific heats	$\gamma = C_p/C_v$	1.40	
Free space sound speed	c	3.47×10^4	cm/s

Denoting by $\lambda(\omega)$ the one-way loss transfer function, and by L/c , the one-way propagation time, the propagation loss is given by $\exp[-j\omega L/c] \cdot \lambda(\omega)$, where

$$\lambda(\omega) = \exp \left[-\alpha(\omega)L - j\omega L(1/\nu(\omega) - 1/c) \right]. \quad (3)$$

An approximation to the phase velocity, valid for all tube radii is [6]

$$\nu(\omega) \approx c \frac{A_v r_v (1 + r_v/\kappa)}{1 + A_v r_v (B_v + r_v/\kappa)}, \quad (4)$$

where r_v is the ratio of the pipe radius a to the thickness of the viscous boundary layer given by

$$r_v = a \left(\frac{\eta}{\omega \rho} \right)^{-\frac{1}{2}}, \quad (5)$$

and the parameters A_v and B_v , given by

$$A_v = \frac{1}{2\sqrt{\gamma}}, \quad B_v = 1 + \frac{[1 + (\gamma - 1)/\nu]}{\sqrt{2}\kappa}, \quad (6)$$

were selected to match the limiting phase velocity behavior, and the parameter

$$\kappa = 2\gamma, \quad (7)$$

marks the ratio r_v delimiting the small-radius and large-radius tube regions [6]. The molecular constants in (5) and (6) are defined in Table I and suggested values are provided.

Similarly, an approximation to the attenuation coefficient is

$$\alpha(\omega) \approx \left(\frac{\omega}{cr_v} \right) \frac{A_\alpha + B_\alpha (r_v/\kappa)}{1 + r_v/\kappa}, \quad (8)$$

where the parameters A_α and B_α were again selected to match the limiting attenuation coefficient behavior and are given by

$$A_\alpha = 2\sqrt{\gamma}, \quad B_\alpha = \frac{[1 + (\gamma - 1)/\nu]}{\sqrt{2}}. \quad (9)$$

Figure 3 shows the approximations for phase velocity and attenuation as given by (4) and (8) along with their complete and limiting behaviors as given by Benade [4].

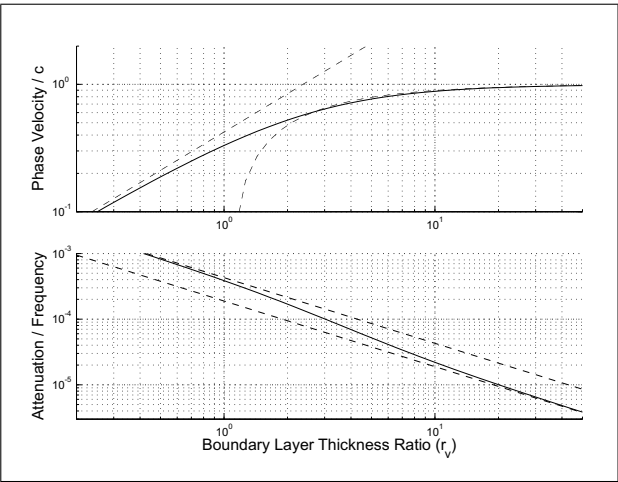


Figure 3. Modeled (solid) phase velocity (top) and attenuation (bottom) and their complete and limiting behavior (dashed).

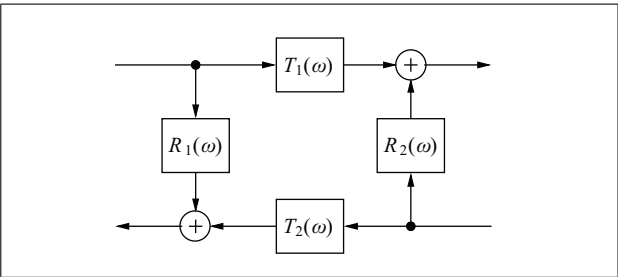


Figure 4. Scattering. A change of impedance may occur as a two-port scattering junction between two waveguide sections consisting of frequency-dependent reflection $R_{1,2}(\omega)$ and amplitude complementary transmission $T_{1,2}(\omega)$.

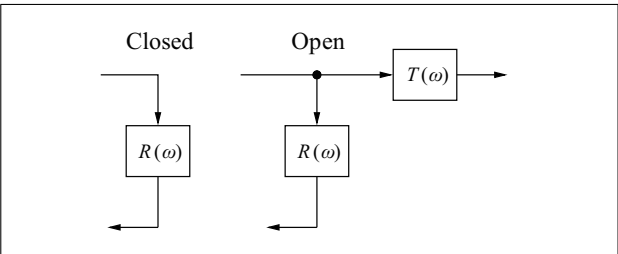


Figure 5. Termination. A change of impedance in a waveguide section may occur as a termination: closed with reflection, or open with a reflection $R(\omega)$ and corresponding complementary transmission.

2.2. Scattering: reflection and transmission

Any change of impedance which may be the result of a termination (either open or closed as discussed in the following section 2.3), a change in the tube’s cross-sectional area, or a connection to another acoustic element, requires filtering to account for the frequency-dependent reflection $R_{1,2}(\omega)$ and amplitude complementary transmission $T_{1,2}(\omega)$ that will result between two adjacent waveguide sections (see Figure 4) or at a termination (see Figure 5).

A change in the wave impedance at the boundary between two tube elements will result in a reflection with transfer function

$$R(\omega) = \frac{Z_2(\omega)/Z_1(\omega) - 1}{Z_2(\omega)/Z_1(\omega)^* + 1}, \quad (10)$$

where Z_1 and Z_2 denote the adjacent wave impedances, and $*$ indicates the complex conjugate. The amplitude complementary transmission transfer function is given by

$$T(\omega) = 1 + R(\omega) \quad (11)$$

for pressure waves [20].

For plane waves in cylindrical tubes (as denoted by the y subscript) the impedance is given by

$$Z_y = \frac{\rho c}{S}, \quad (12)$$

where S is the cross-sectional area of the tube.

For spherical pressure waves in conical tubes (as denoted by the n subscript) propagating away from the cone apex (denoted by the $+$ superscript), the impedance is dependent on frequency ω and the distance r from the observation point to the cone apex, and is given by

$$Z_n^+(r; \omega) = \frac{\rho c}{S} \frac{j\omega}{j\omega + c/r}. \quad (13)$$

For spherical waves propagating toward the cone apex, the impedance is given by

$$Z_n^-(r; \omega) = \frac{\rho c}{S} \frac{j\omega}{j\omega - c/r} = Z_n^{+*}(r; \omega). \quad (14)$$

2.3. Termination: reflection and transmission

A special case of a change in cross section is at the instrument's open end. In this case, the complex terminating impedance $Z_2(\omega) = Z_L(\omega)$, may be a complicated function of frequency. In the case of a cylindrical tube, an expression is available by Levine and Schwinger in terms of Bessel and Struve functions [21]. There is no known expression for conical bores.

The ratio Z_L/Z_1 may be approximated by

$$Z_L/Z_1 \approx \frac{jka}{\zeta + jka}, \quad (15)$$

where $k = \omega/c$ is the wavenumber, a is the radius of the cylinder, and ζ is a scalar near one which determines the transition between the low-frequency and high-frequency behaviour. The expression (15) follows the gross behaviour described by Levine and Schwinger. The reflection filter for the open end on a cylindrical tube may then be approximated by

$$R_{op}(\omega) = \frac{Z_L/Z_1 - 1}{Z_L/Z_1 + 1} = \frac{-1}{1 + 2jka/\zeta}, \quad (16)$$

yielding a one-pole low-pass filter with a cutoff frequency of $\omega = \zeta c/a$.

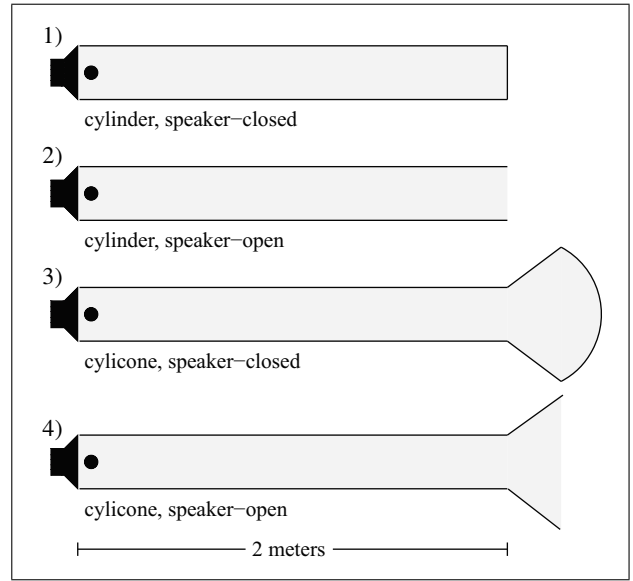


Figure 6. Four simple tube structures, each terminated at one end with a speaker and having a co-located microphone. The following terminations are applied at the end opposite the speaker and microphone: 1) a cylinder closed with Lucite to ensure a perfect reflection (cylinder, speaker-closed), 2) an open cylinder (cylinder, speaker-open), 3) a cylicone terminated with a glass sphere (with radius nearly that of the cone) ensuring a perfect reflection of spherical waves (cylicone, speaker-closed), 4) an open cylicone (cylicone, speaker-closed).

3. Measurement configuration

To isolate each of the waveguide model elements seen in Figure 1, a test signal, a swept sinusoid similar to that described by Farina [16], was input through a speaker at one end of four tube configurations: a cylindrical tube, and the cylinder with an attached conical flare (cylicone), each measured with the end opposite the speaker closed, then open (see Figure 6).

1. **Cylinder, closed end.** A two-meter-long cylinder is rigidly terminated at one end to ensure a perfect reflection. This configuration allows measurement of the speaker output $\sigma(\omega)$, the speaker reflection $\rho(\omega)$, and the wall loss $\lambda(\omega)$ transfer functions, as described in section 4.1. The arrival responses L_n for this measurement may be seen in Figure 7.
2. **Cylinder, open end.** Opening the cylinder allows measurement of the reflection at the open end of a cylinder, $R_{op}(\omega)$, as described in section 4.2. Figure 9 shows the measured responses.
3. **Cylicone, closed end.** The addition of a conical flare with a spherical termination (to ensure a perfect reflection) to the above cylindrical tube allows reflection and transmission at the junction to be observed from the measured responses shown in Figure 11, as described in section 4.3.
4. **Cylicone, open end.** Opening the conical end allows us to observe the corresponding reflection from the cylicone response shown in Figure 13, as described in section 4.4.

As described below, by using a long swept sinusoid to obtain a system impulse response for each structure, the system is excited with sufficient energy to achieve a significantly larger SNR than could be obtained with a simple pulse, while achieving the bandwidth of interest, in this case up to 10 kHz. The impulse responses measured here have a peak level roughly 70 dB above the noise floor standard deviation. There is no limit to the duration of the swept sinusoid, i.e. its length is not bounded by the microphone placement, the length of the tube or any other potential for overlap between signal and reflections seen in other methods, since the signal recorded at the microphone is processed to produce the response of the system had it been excited with a pulse only one sample long.

The test signal used was a sinusoid exponentially swept from 20 Hz to the band edge of 22.05 kHz (half the sampling rate, f_s), and with a duration of 2^{20} samples, or about 23 seconds. Expressed mathematically, the sine sweep is given by

$$s(t) = \sin(\phi(t)), \quad \phi(t) = \int_0^t \omega(\tau) d\tau, \quad (17)$$

where the frequency $\omega(t)$ traces out an exponential sweep,

$$\omega(t) = 2\pi f_0 e^{\eta t}, \quad (18)$$

where $\eta = \ln(f_0/2f_s)/T$, with f_s being the sampling rate, f_0 the initial frequency, and T the duration of the sweep.

A sine sweep was repeated so that the measured response during the second sweep would be the circular convolution of the input sweep with the system. In particular, to recover the system impulse response from the sweep response, circular deconvolution may be used. Denoting by $r(t)$ the system response during the second sweep, we have

$$\hat{h}(t) = \mathcal{F}^{-1} \{ \mathcal{F}r(t) / \mathcal{F}s(t) \}. \quad (19)$$

where \mathcal{F} denotes the Fourier Transform. Expressed in Matlab code, the impulse response \mathbf{h} may be found with

$$\mathbf{h} = \text{ifft}(\text{fft}(\mathbf{r}) ./ \text{fft}(\mathbf{s})); \quad (20)$$

where \mathbf{s} contains the sine sweep and \mathbf{r} is the system response during the second sine sweep.

The input signal and the measured response is sent and received simultaneously using a full duplex audio device; in this work the Mac PowerBook running Logic Pro with the MOTU Traveler audio interface, with 16-bit audio at a sampling rate of 44.1 kHz was used. Measurements were taken in a very large room with the apparatus placed five meters from the nearest reflecting object.

The four simple tube structures in Figure 6 were assembled using PVC tubes and plastic funnels of several sizes. The cylinder was prepared by placing a speaker (CUI Inc. CMS0281KLX) at one end, and by press fitting a six-millimeter-diameter microphone (Panasonic W64M) into a hole drilled next to the speaker. It is not necessary to consider or document the precise details of the speaker

and microphone as long as their placement and geometry is consistent from one measurement to the next. Any effects of placement and geometry are eliminated by the signal normalization and post processing described in the following section. It is important however, that the microphone and speaker be placed as close as possible to each other to minimize the acoustic travel time between them. In this way the corresponding frequency at which destructive interference occurs between the signal traveling from speaker to microphone and that returning from the bore is made large. Destructive interference will result in a notch in the transfer function and will impact the ability to take the spectral ratios described in section 4 at that frequency. In this case, the distance between the microphone and speaker is sufficiently small to ensure that any spectral nulls would be outside the 10 kHz band of interest.

The cylinder is 2 m long, with an inside radius $a = 1$ cm, and the cone is 12.7 cm long with edge radii of $a_1 = 1$ cm, and $a_2 = 9.2$ cm. Both cylinder and cone are sufficiently thick to be considered rigid (3 mm and 2 mm, respectively).

The impulse response between the speaker and microphone was measured for each of the configurations. The impulse responses were then equalized according to the first arrival, the speaker-microphone transfer function $\sigma(\omega)$, to produce the figures shown in section 4. Note that the first arrival will also contain contributions from evanescent modes, in this case above about 10 kHz.

4. Measured responses

In spite of the wide use of digital waveguides for sound synthesis, it is perhaps less common to observe the behaviour of wave propagation in actual acoustic systems from the same perspective. That is, rather than analyzing a system purely from its frequency response, it is informative for analysis, and practical for synthesis, to observe the effects of each waveguide element in a sequence of multiple arrivals comprising the system impulse response.

4.1. Closed cylinder

A first measurement is taken for the cylinder closed at the end opposite the speaker, ensuring a perfect reflection. Comparing arrivals appearing in its impulse response provides estimates of the propagation loss $\lambda(\omega)$, speaker transfer function $\sigma(\omega)$ and the speaker reflection function $\rho(\omega)$.

The first four arrivals comprising the measured speaker-microphone impulse response are shown in Figure 7. The direct path speaker-microphone response is observed as a positive pulse labeled L_1 at $t \approx 2.5$ ms and corresponds to the equalized transfer function $\sigma(\omega)$. (Note that the 2.5 ms arrival time corresponds to buffering delays between the sweep and response in the measurement system.) This energy propagates down the length of the tube and is perfectly reflected from the closed end, returning to the speaker and co-located microphone at $t \approx 14$ ms. The

arrival L_2 is reflected from the speaker, and the observed pulse L_2 is the sum of the incoming and speaker-reflected waves. The pulse makes another round trip, eventually producing the sequence of consecutive equally spaced pulses observed in Figure 7. There is an attenuation of the pulse upon each successive reflection. There is also an observable low-pass filtering, as the signal becomes increasingly smooth and widened with every reflection (Figure 7).

Given the arrival responses for a closed cylinder, L_n , the transfer function of the reflection from the speaker may be estimated. The first arrival, which is the output of the speaker measured at the mic, consists solely of the speaker transfer function:

$$L_1 = \sigma(\omega). \tag{21}$$

The following arrival, L_2 , consists of the sum of left and right traveling pressure waves at the microphone position: the speaker transfer function after having travelled twice the length of the tube (round trip), given by $L_2^- = \sigma(\omega)\lambda^2(\omega)$, and the speaker transfer function with round trip losses after reflecting from the speaker, $L_2^+ = \sigma(\omega)\lambda^2(\omega)\rho(\omega)$. The second arrival is expressed as their sum, and is given by

$$L_2 = L_2^+ + L_2^- = \sigma(\omega)\lambda^2(\omega)(1 + \rho(\omega)). \tag{22}$$

Each subsequent arrival for the closed cylinder consists of the previous arrival, with round-trip wall losses of $\lambda^2(\omega)$ and a speaker reflection $\rho(\omega)$. The third arrival is therefore given by

$$L_3 = \sigma(\omega)\lambda^4(\omega)\rho(\omega)(1 + \rho(\omega)). \tag{23}$$

These three responses are sufficient for defining the intermediate variable

$$\zeta(\omega) = \frac{L_1 L_3}{(L_2)^2} = \frac{\rho(\omega)}{1 + \rho(\omega)}, \tag{24}$$

which yields an estimate for the speaker reflection transfer function,

$$\hat{\rho}(\omega) = \frac{\zeta(\omega)}{1 - \zeta(\omega)}, \tag{25}$$

and the propagation loss $\lambda(\omega)$,

$$\hat{\lambda}^2(\omega) = \frac{L_3}{\hat{\rho}(\omega)L_2}. \tag{26}$$

Figure 8 shows the estimated and theoretical propagation loss along with the estimated speaker reflection. Note the good agreement between the estimated and theoretical propagation losses. The low-frequency attenuation observed in the spectrum of the speaker reflection is likely due to the speaker being designed to be resonant at low frequencies. It should be pointed out that there is roughly a fraction of a dB attenuation in the estimated propagation loss beyond that theoretically predicted.

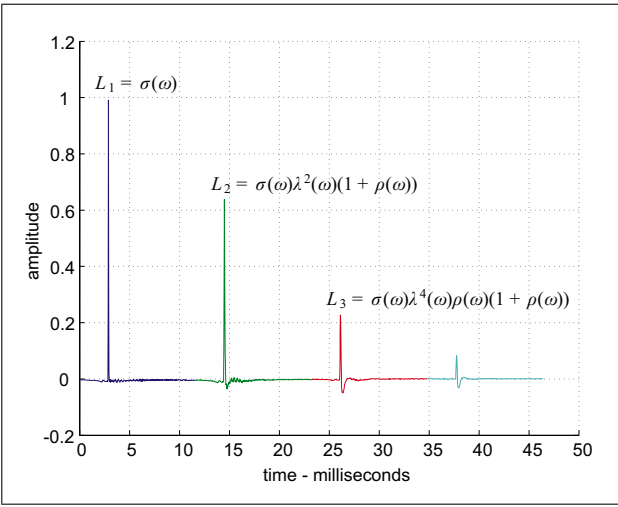


Figure 7. Arrival responses for the closed cylinder, showing individual pulses and corresponding spectra as combinations of transfer functions for the speaker $\sigma(\omega)$, wall losses $\lambda(\omega)$, and speaker reflection $\rho(\omega)$.

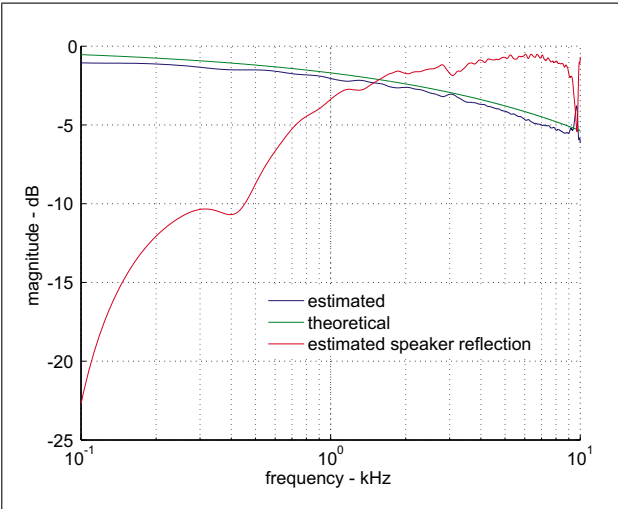


Figure 8. Theoretical (upper smooth curve) and estimated (lower curve 0.5 dB down) propagation losses along with the estimated speaker reflection (high-pass curve).

4.2. Open cylinder

The open-end reflection transfer function $R_{op}(\omega)$ may be estimated from the open cylinder impulse response shown in Figure 9. The low-pass characteristic described by Levine and Schwinger is apparent in the successive arrivals, which are increasingly smeared over time compared to their closed-end counterpart shown in Figure 7. Successive arrivals show the same propagation delay as observed for the closed cylinder, but in this case with every other reflection inverted, and with increased attenuation and low-pass filtering with each consecutive reflection (Figure 9). This is expected as the responses Y_n have all the losses of the closed cylinder (propagation and speaker reflection losses) with the added effect of the open-end reflection.

As with the closed cylinder, the initial response of this measurement is merely the response of the speaker to an

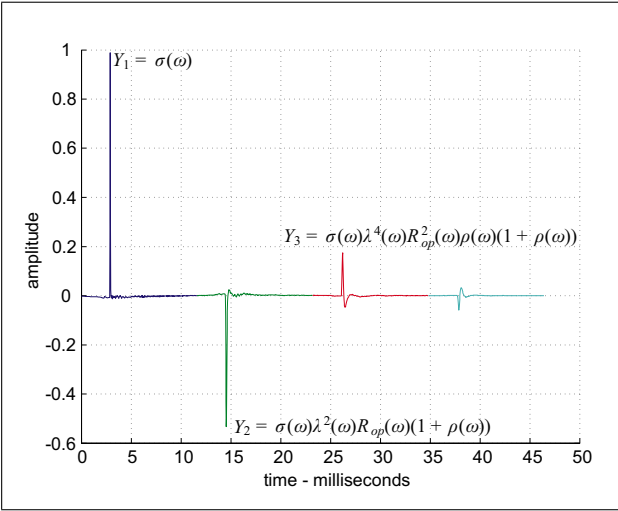


Figure 9. Measured impulse response for the open cylinder showing individual arrivals. The open-end transfer function $R_{op}(\omega)$ may be isolated by comparison with the corresponding closed-end arrival spectra L_2, L_3, L_4 .

impulse, yielding the speaker transfer function, $Y_1 = \sigma(\omega)$. The second arrival, Y_2 , is similar to L_2 but also includes the open-end reflection

$$Y_2 = \sigma(\omega)\lambda^2(\omega)R_{op}(\omega)(1 + \rho(\omega)). \tag{27}$$

Subsequent arrival responses include additional round-trip wall losses and open-end reflections. The open-end reflection function may then be estimated as the ratio of the second arrival spectra,

$$\hat{R}_{op}(\omega) = \frac{Y_2}{L_2}, \tag{28}$$

and is seen in Figure 10.

4.3. Closed cylicone

Attaching a conical flare to the cylindrical tube, and terminating with a spherical cap to ensure a perfect reflection, allows for estimation of the reflection and transmission filters associated with the junction.

Figure 11 shows the measured impulse response, including groups of arrivals resulting from energy reflected between the end cap and the junction. Consider the individual *subarrivals* within the second arrival group A_2 of Figure 11. The signal from the speaker propagates along the length of the cylinder to the junction, where part of the signal is reflected back to the microphone and inverted (as can be seen from (10) where if $Z_1(\omega) > Z_2(\omega)$, the reflection $R(\omega)$ picks up a negative sign). It appears as the negative pulse $A_{2,1}$, with losses having a low-pass characteristic described by $R_y(\omega)$, as well as round-trip wall losses given by $\lambda_y^2(\omega)$. The part of the signal that is not reflected is transmitted through the junction, with losses having a complementary high-pass characteristic $T_y(\omega)$. This signal propagates to the spherical termination where it is “perfectly” reflected, arriving back at the junction a short

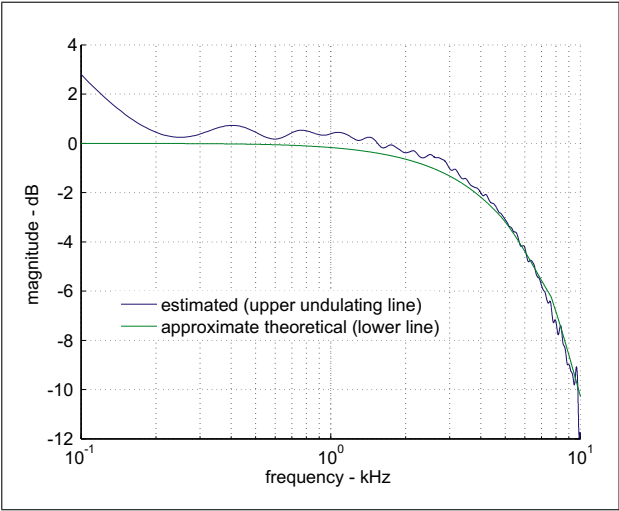


Figure 10. Estimated and approximate theoretical open-end cylinder reflection magnitude. The theoretical reflection magnitude is a first-order approximation that captures the general low-pass characteristic. Note that the estimated reflection magnitude is greater than one at low-frequencies where the speaker doesn’t generate significant power and more measurement noise is introduced. The measurement matches the approximate theoretical curve above 2 kHz and within a fraction of a dB otherwise.

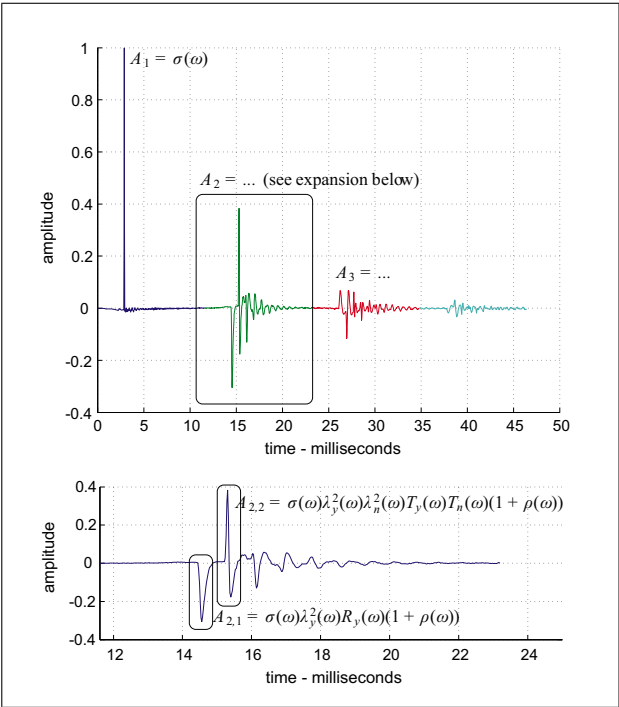


Figure 11. Arrival responses are shown with their corresponding transfer functions. The response $A_{2,1}$ shows a low-pass characteristic expected of a junction reflection, while $A_{2,2}$ shows a high-pass characteristic expected of two transmissions through the junction.

time later (corresponding to twice the length of the cone). Part of this signal at the junction is transmitted with transfer function $T_c(\omega)$, producing the pulse at $t \approx 15$ ms ($A_{2,2}$ in Figure 11), and part is reflected, with transfer function

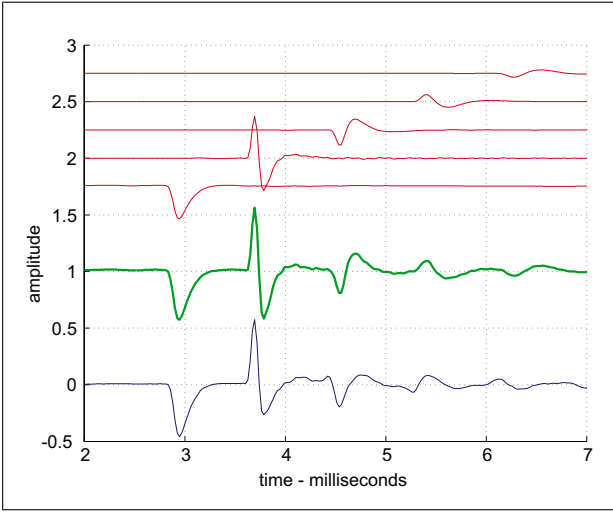


Figure 12. Measured (lower line), theoretical (thick line offset by 1.0) and components (upper lines offset by 0.25) for closed cone second arrival group, corresponding to $A_{2,i}$.

$R_c(\omega)$. Note the doublet nature of the pulse $A_{2,2}$, with the steep transition from a positive to a negative peak being consistent with the high-pass transmission through the junction. The part of the pulse reflected back toward the end cap will appear at the junction to be in part transmitted to the cylinder and microphone, and in part reflected once again toward the end cap.

The first subarrival spectrum is

$$A_{2,1} = \sigma(\omega)\lambda_y^2(\omega)R_y(\omega)(1 + \rho(\omega)). \quad (29)$$

with subsequent i^{th} arrivals having spectrum

$$A_{2,i} = \sigma(\omega)\lambda_y^2(\omega)\lambda_n^{2i}(\omega) \cdot T_y(\omega)T_n(\omega)R_n^{i-1}(\omega)(1 + \rho(\omega)). \quad (30)$$

The individual subarrivals shown in Figure 12 were generated according to (30) using the transmission and reflection filters described in section 2 for the 45° cone and one-centimeter radius cylinder measured. The subarrivals are summed to form the theoretical arrival group shown in Figure 12. Note the good agreement between the theoretical and measured responses. It should be pointed out that the estimation of the junction transmission and reflection filters in this case is complicated somewhat by the overlapping nature of the subarrivals. Rather than fix the reflection and transmission filters by analyzing individual arrivals, hypothesized filters are used to generate the entire arrival group and then adjusted to produce the group best matching the one measured.

4.4. Open cylicone

Opening the end of the cone produces an impulse response with similar behaviour as for the closed cylicone, though, because it is open, the cone termination reflections are inverted and attenuated. A positive pulse traveling from the speaker to the junction is partly inverted upon reflection,

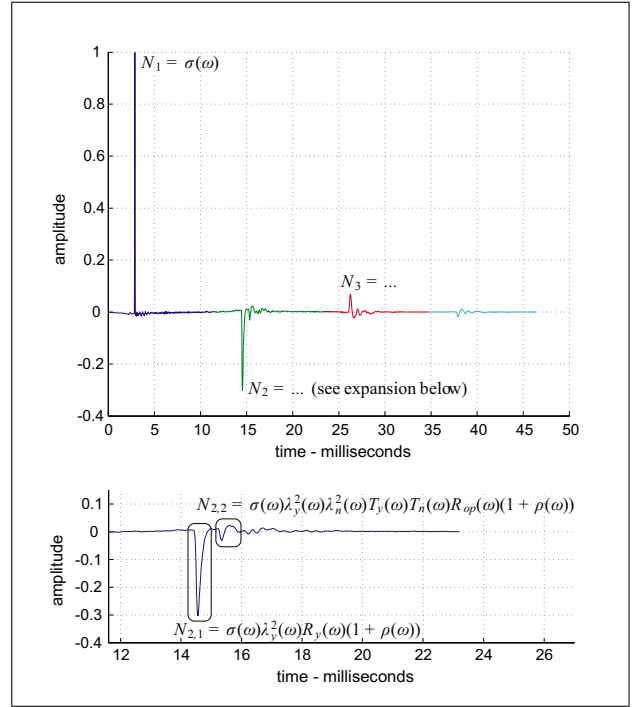


Figure 13. Arrival responses for the open cylicone showing individual pulses corresponding to outputs of a combinations of transfer functions.

arriving at the microphone as a negative pulse, and partly transmitted through the junction, this time being inverted at the open cone termination reflection. When the negative pulse arrives at the junction, a part is transmitted as a negative pulse to the microphone, and a part is reflected as a positive pulse back to the open cone termination where it is again inverted, becoming negative. The negative pulse propagates back to the junction where it is partly transmitted to the microphone, and partly reflected and inverted, and so on.

Figure 13 shows the measured impulse response for the open cylicone. Like the closed cylicone, it exhibits a sequence of arrival groups. The N_2 subarrival spectra may be written in terms of the closed cylicone subarrival spectra,

$$N_{2,i} = A_{2,i}R_{op}^{i-1}(\omega). \quad (31)$$

Approximating the reflection from the open cone as a first-order low-pass filter, with characteristic closely matching both observed measurement and that described by Levine and Schwinger (15) for a cylindrical radius equal to the average of the cone's edge radii a_1 and a_2 , a theoretical arrival response is shown in Figure 14 along with its component subarrivals and the measured N_2 arrival group. As in the case of the closed cylicone there is good agreement between the measured and theoretical responses.

5. Results and conclusions

In this work, a measurement technique was presented for estimating elements comprising a waveguide wind instru-

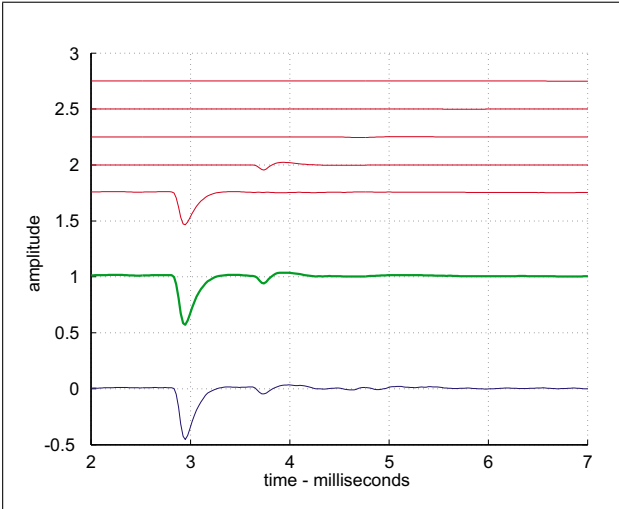


Figure 14. Measured (lower line), theoretical (thick line offset by 1.0) and components (upper lines offset by 0.25) for the open cone second arrival, corresponding to $N_{2,2}$.

ment model, including filters used in propagation, scattering, and termination. The technique measures the impulse response between the mouthpiece end of the instrument and a co-located microphone. By comparing corresponding arrivals for different configurations, modeled reflection, transmission, and loss filters may be identified. To validate the measurement technique, it was applied to a simple instrument configuration having a cylindrical bore connected to a conical bell. The estimated filters and impulse response was seen to closely match the theory, giving confidence that the measurement method can be generally applied.

To confirm the good agreement between the measured and theoretical reflection, transmission, and propagation elements, waveguide models of the four tube configurations were implemented based on cylinder and cone dimensions. Figure 15 shows a close match between measured and theoretically-derived waveguide model impulse responses for each of the tube configurations.

This work will facilitate the development of filter components for which theoretical solutions may not be available. In particular, reflection and transmission functions of wind instrument bores, bells, and mouthpieces can be measured by comparing the response of a rigidly terminated tube to that of the tube with the instrument, or instrument section, affixed.

Acknowledgments

We would like to sincerely thank Theresa Leonard and the Banff Centre for the Arts for the use of their facilities, John Lundell, Carr Wilkerson, Michael Coury, and Harrison Smith for their help in fabricating the experimental setup, and the Natural Sciences and Engineering Research Council of Canada (NSERC) for their support. Many thanks are also extended to the reviewers whose careful reading of this text, and invaluable comments, have greatly strengthened the clarity and accuracy of this work.

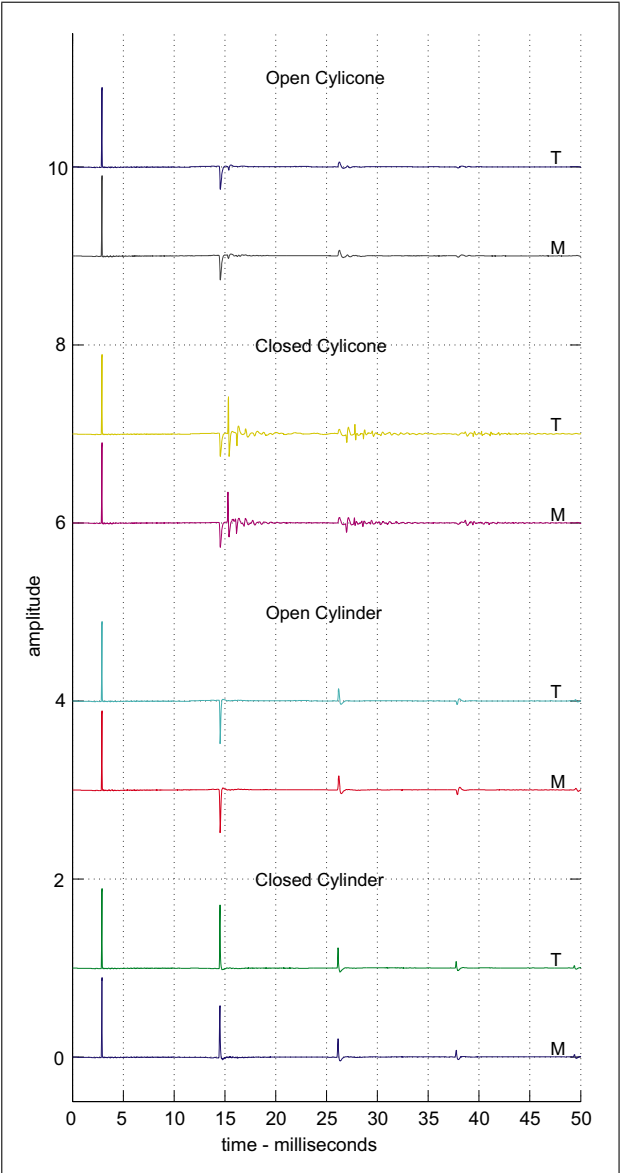


Figure 15. Measured and theoretically-derived impulse response for (from bottom to top) a closed cylinder, an open cylinder, a closed cylicone, and an open cylicone.

References

- [1] J. O. Smith: Digital waveguide modeling of musical instruments. www-ccrma.stanford.edu/~jos/waveguide/, 2003. last viewed 12/4/2008.
- [2] V. Välimäki: Discrete-time modeling of acoustic tubes using fractional delay filters. Dissertation. Helsinki University of Technology, Faculty of Electrical Engineering, Laboratory of Acoustic and Audio Signal Processing, Espoo, Finland, 1995. Report no. 37.
- [3] D. P. Berners: Acoustics and signal processing techniques for physical modeling of brass instruments. Dissertation. Stanford University, Stanford, California, July 1999.
- [4] A. H. Benade: On the propagation of sound waves in a cylindrical conduit. *Journal of the Acoustical Society of America* **44** (1968) 616–623.
- [5] D. H. Keefe: Acoustical wave propagation in cylindrical ducts: Transmission line approximation for isothermal and

- nonisothermal boundary conditions. *Journal of the Acoustical Society of America* **75** (January 1984) 58–62.
- [6] J. Abel, T. Smyth, J. O. Smith: A simple, accurate wall loss filter for acoustic tubes. DAFX 2003 Proceedings, London, UK, September 2003, International Conference on Digital Audio Effects, 53–57.
- [7] X. Rodet, C. Vergez: Physical models of trumpet-like instruments: Detailed behavior and model improvements. Proceedings of ICMC 1996, Clear Water Bay, Hong-Kong, August 1996, International Computer Music Conference.
- [8] A.H.Benade, M.I.Ibisi: Survey of impedance methods and a new piezo-disk-driven impedance head for air columns. *Journal of the Acoustical Society of America* **81** (April 1987) 1152–1167.
- [9] J.Kergomard, R.Caussé: Measurement of acoustic impedance using a capillary: An attempt to achieve optimization. *Journal of the Acoustical Society of America* **79** (April 1986) 1129–1140.
- [10] T. Ossman, H. Pichler, G. Widholm: Bias: A computer-aided test system for brass wind instruments. Audio Engineering Society Preprint, October 1989.
- [11] J. Epps, J.R.Smith, J.Wolfe: A novel instrument to measure acoustic resonances of the vocal tract during phonation. *Measurement Science and Technology* **8** (July 1997) 1112–1121.
- [12] M. M. Sondhi, J. Resnick: The inverse problem for the vocal tract: Numerical methods, acoustical experiments, and speech synthesis. *Journal of the Acoustical Society of America* **73** (March 1983) 985–1002.
- [13] J. Agulló, S. Cardona, D. H. Keefe: Time-domain deconvolution to measure reflection functions for discontinuities in waveguides. *Journal of the Acoustical Society of America* **97** (March 1995) 1950–1957.
- [14] V. Välimäki, B. Hernoux, J. Huopaniemi, M. Karjalainen: Measurement and analysis of acoustic tubes using signal processing techniques. Finnish Signal Processing Symposium (FINSIG'95), Espoo, Finland, June 1995.
- [15] D. B. Sharp: Acoustic pulse reflectometry for the measurement of musical wind instruments. Dissertation. University of Edinburgh, 1996.
- [16] A. Farina: Simultaneous measurement of impulse response and distortion with a swept-sine technique. Proceedings of the 108th AES Convention, Paris, France, February 2000, 18–22.
- [17] A. Lefebvre, G. Scavone, J. Able, A. Buckiewicz-Smith: A comparison of impedance measurements using one and two microphones. Proceedings of ISMA 2007, Barcelona, Spain, September 2007, International Symposium on Musical Acoustics.
- [18] A. Lefebvre: La mesure de l'impédance acoustique du saxophone alto. Diploma Thesis. École Polytechnique de Montréal, 2006.
- [19] T. Smyth, J. Abel: Convolutional synthesis of wind instruments. Proceedings of the IEEE Workshop on Applications of Signal Processing to Audio and Acoustics (WASPAA'07), New Paltz, New York, October 2007.
- [20] J. O. Smith: Physical audio signal processing for virtual musical instruments and audio effects. December 2008, <http://ccrma.stanford.edu/~jos/pasp/>.
- [21] H. Levine, J. Schwinger: On the radiation of sound from an unflanged circular pipe. *Phys. Rev* **73** (1948) 383–406.